Calmodulin interactions with Ca_V1 and Ca_V2 voltage-gated calcium channel IQ domains

Eun Young Kim[†], *Felix Findeisen*[†] *and Daniel L Minor*[†,‡,§,§§]

[†] Cardiovascular Research Institute, University of California, San Francisco, CA 94158-2330, USA [‡] Departments of Biochemistry and Biophysics, and Cellular and Molecular Pharmacology, University of California, San Francisco, CA 94158-2330, USA [§] California Institute for Quantitative Biomedical Research, University of California, San Francisco, CA 94158-2330, USA [§§] Physical Biosciences Division, Lawrence Berkeley National Laboratory, Berkeley, CA 94720, USA

FUNCTIONAL CLASS

Calcium binding protein: Calmodulin (CaM) is a bilobed, 16.7-kDa calcium binding protein involved in intracellular Ca^{2+} signaling[1] and is a member of a larger family of calcium sensor proteins.[1,2] CaM contains two pairs of independently folded domains[3,4] that each contain two Ca^{2+} binding motifs known as *EF hands*,[5,6] each of which can bind a single Ca^{2+} ion. Ca^{2+} binding to the EF-hand pairs causes a conformational change in the individual lobes, which exposes a phenylalanine and methionine-rich hydrophobic pocket[7,8] that allows Ca^{2+}/CaM to interact with more than 300 different target proteins in a variety of binding modes.[1,8,9] CaM directly modulates numerous types of ion channels.[10]

Ion channel: Voltage-gated calcium channels (Ca_Vs)[11,12] are transmembrane ion channels found throughout metazoan life[11,13–15] and are members of the superfamily of voltage-gated ion channels[16,17] that constitutes the third most abundant set of genes in the human genome.[17] There are two Ca_V functional classes that have diverse physiological and pharmacological properties: high-voltage-activated Ca_Vs (Ca_V1s and Ca_V2s),[11] which open in response to strong membrane depolarization (~+30 to +50 mV), and low-voltage-activated Ca_Vs (Ca_V3s), which open in response to weaker membrane depolarization (~−55 to −20 mV).[18,19] The high-voltage-activated class is further divided on the basis of both pharmacology and functional properties into L-type (Ca_V1s)[13,20] and non-L-type (Ca_V2s)[13,21,22] channels (Table 1).

The Ca_V1 and Ca_V2 functional unit comprises four separate subunits (Figure 1(a) and (b)) that have a total molecular mass >0.5 MDa[28] and include a transmembrane, pore-forming subunit ($Ca_V\alpha_1$) that contains four homologous repeats composed of six transmembrane segments each (Figure 1(b)) and that sets many of the functional and pharmacological properties of the channel[11,13] (Table 1); a cytoplasmic subunit ($Ca_V\beta$) that shapes channel inactivation properties and regulates plasma membrane expression[29]; a membrane-anchored subunit ($Ca_V\alpha_2\delta$) that is the receptor for antiepileptic and antinociceptive drugs[30]; and calmodulin (CaM).[31] CaM acts as an intrinsic calcium sensor that endows the channels with strong calcium-dependent responses known as *calcium-dependent inactivation* (*CDI*) and *calcium-dependent facilitation* (*CDF*).[32,33] The central site of the CaM interactions that govern CDI and CDF is an IQ domain present in the $Ca_V\alpha_1$ C-terminal cytoplasmic tail (Figure 1(c)).[24,26,27,34–37] Interactions between

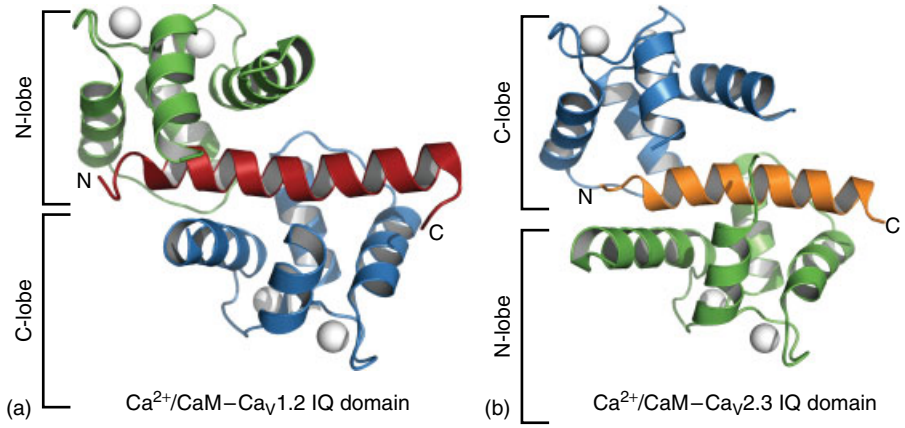

3D Structure Cartoon representation of Ca^{2+}/CaM complexes with the IQ domains from representative Ca_V1 (a) 2BE6 and Ca_V2 (b) 3DVK. Ca^{2+}/CaM N-lobe and C-lobe are displayed in green and blue, respectively. The white spheres are calcium ions. All structural figures were prepared using PyMOL.[101]

Table 1 Ca_V nomenclature and Ca^{2+}/CaM–IQ domain complexes

Native channel		Pore-forming $Ca_V\alpha_1$ subunit		Ca^{2+}/CaM–IQ domain complexes						
		Classification		Resolution (Å)	Peptide length (amino acids)	Residues	IQ numbers	Source	PDB code	References
		Alphabetical	Numerical							
L-type		α_{1S}	$Ca_V1.1$	1.94	21	1522–1542	I1529/Q1530	Human	2VAY	23
		α_{1C}	$Ca_V1.2$	2.00	34	1611–1644	I1624/Q1625	Human	2BE6	24
				1.45	21	1655–1685	I1672/Q1673	Human	2F3Y	25
				1.60	21	IQ → AA mutant 1655–1685	I1672A/Q1673A	Human	2F3Z	25
		α_{1D}	$Ca_V1.3$				N/A			
		α_{1F}	$Ca_V1.4$				N/A			
Non-L-type	P/Q-type	α_{1A}	$Ca_V2.1$	2.60	25	1963–1984	I1971/M1972	Rabbit	3DVM	26
				2.60	21	1960–1980	I1967/M1968	Human	3BXK	27
	N-type	α_{1B}	$Ca_V2.2$	2.35	25	1855–1876	I1863/F1864	Rabbit	3DVE	26
				2.80	25	1853–1876	I1863/F1864	Rabbit	3DVJ	26
	R-type	α_{1E}	$Ca_V2.3$	2.30	25	1818–1839	I1826/M1827	Rat	3DVK	26
				2.20	21	1819–1839	I1826/M1827	Human	3BXL	27

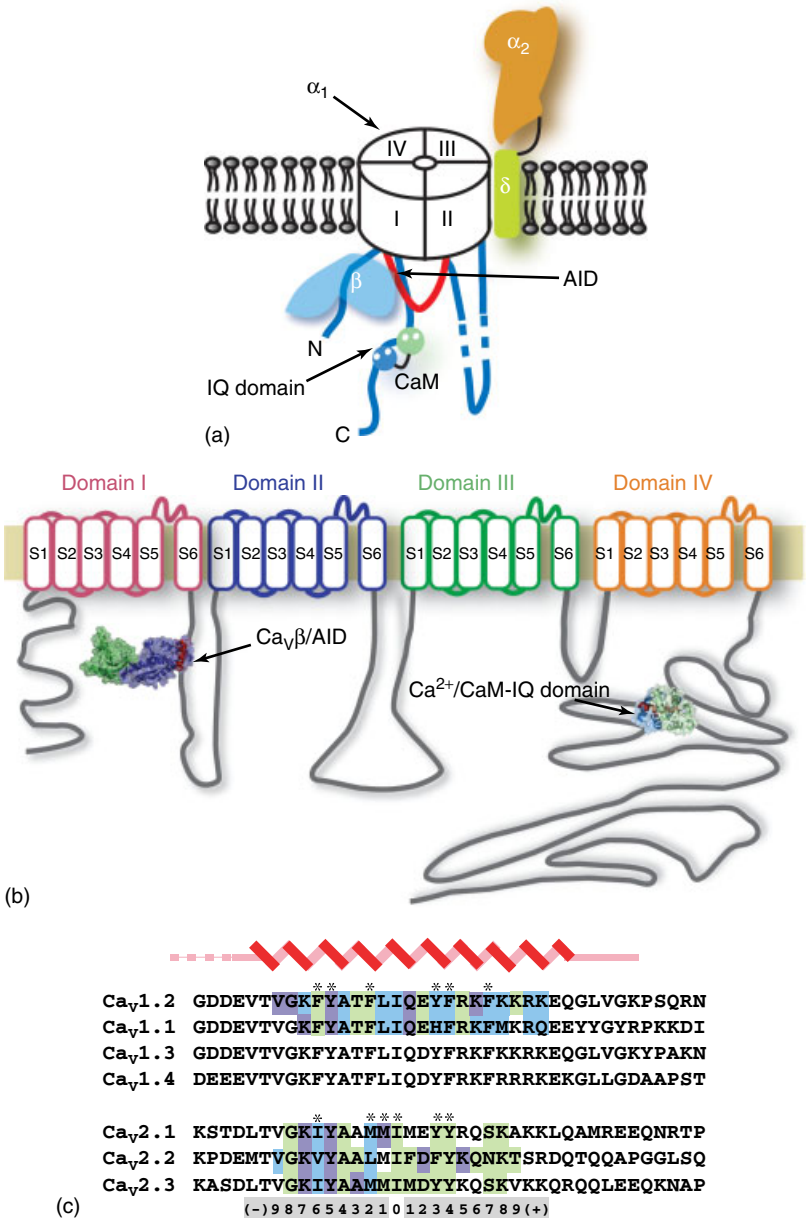

Figure 1 Voltage-gated calcium channel structure and IQ domain comparison. (a) Cartoon diagram of a Ca_V1 or Ca_V2 channel. The four homologous transmembrane domains of $Ca_V\alpha_1$ are indicated. $Ca_V\beta$ is shown in blue and interacts with its high-affinity binding site on the I–II intracellular loop known as the α-*interaction domain* (*AID*). CaM is shown bound to the C-terminal cytoplasmic tail at the site of the IQ domain. The $Ca_V\alpha_2\delta$ membrane-associated subunit is shown in orange and green. (b) Topology of the pore-forming $Ca_V\alpha_1$ subunit. Positions of the $Ca_V\beta$/AID complex (PDB: 1T0J)[38] and Ca^{2+}/CaM–IQ domain (PDB: 2BE6)[24] complexes are shown. (c) Comparison of the IQ domain sequences from Ca_V1 and Ca_V2 channels. Positions of main anchors are indicated by the asterisks. Colors indicate contacts to the N-lobe (green), C-lobe (blue), or both (purple). Sequence positions relative to Ile(0) of the IQ motif is shown.

Ca^{2+}/CaM and IQ domains from various Ca_V1 and Ca_V2 subtypes have recently been intensely scrutinized by crystallographic, biochemical, and functional studies.[24–27]

OCCURRENCE

CaM is found in all eukaryotic cells[39–42] and is one of the most highly conserved protein sequences known[8,40,42] (see reference 43 for a detailed comparison of CaM sequences). In mammalian cells, a single isoform of CaM is encoded by multiple genes.[42,44]

Ca_Vs are present in all metazoans.[13] Besides numerous vertebrate examples, phylogenetic comparison indicates that Ca_Vs are ancient molecules that have features conserved between mammals and invertebrates such as sea squirts,[15] *Drosophila*,[45,46] *Caenorhabditis elegans*,[47,48] coral,[49] and jellyfish.[50] The different Ca_V subtypes have

particular tissue and subcellular distributions. $Ca_V1.1$ is most abundant in skeletal muscle[13] and is directly coupled to the ryanodyne receptor intracellular calcium-release channel.[51] $Ca_V1.2$ is present in the brain, heart, smooth muscle, and endocrine cells.[13,20,52,53] $Ca_V1.3$ is important in sensory cells, such as cochlear hair cells and photoreceptors, neuroendocrine cells, the sinoatrial node of the heart, and neurons.[13,20,52–54] $Ca_V1.4$ is largely restricted to the retina.[13,20,55,56] $Ca_V2.1$, $Ca_V2.2$, and $Ca_V2.3$ are found throughout the central and peripheral nervous systems.[13,21,22,57] In particular, $Ca_V2.1$ and $Ca_V2.2$ play key roles in the modulation of neurotransmitter release.[21,22] Ca_Vs have a multitude of splice variants. In a number of cases, the resulting amino acid differences have been shown to provide functional diversification that may tailor Ca_V function to particular environments and specialized cell types.[56,58,59]

BIOLOGICAL FUNCTION

Ca_Vs are the molecules that define excitable cells.[16] Calcium ion influx has two major effects: it depolarizes the cell membrane and increases the intracellular concentration of calcium ions which can act as chemical signal effectors.[39] Therefore, Ca_Vs act as a nidus for cross talk between electrical and chemical signals. Consequently, they have prominent roles in the function of nerve and muscle[11,13,21,57] and also play important roles in hormone secretion from adrenal[52] and pancreatic cells.[53] Mutations in Ca_Vs are linked to a wide range of human diseases and syndromes that include hypokalemic periodic paralysis ($Ca_V1.1$)[55]; cardiac arrhythmias and autism ($Ca_V1.2$)[60]; stationary night blindness ($Ca_V1.4$)[55,56]; and migraine ($Ca_V2.1$).[61] Because of their critical role in human physiology, both L-type[62,63] and non-L-type channels[64,65] are the targets for a wide range of drugs. These include dihydropyridines, phenylalkylamines, diltiazem, and mibefradil that are used to treat cardiovascular diseases including angina, arrhythmias, congestive heart failure, and hypertension,[66–68] and drugs for epilepsy and chronic pain.[69–71]

AMINO ACID SEQUENCE INFORMATION

Calmodulin (CaM)

- *Saccharomyces cerevisiae:* isoform 1 (canonical CaM), 147 amino acid residues (AA), SWISSPROT Id code (SWP) P06787.[72]
- *Homo sapiens*: isoform 1, 148 AA, SWP P62158.[73]
- *Chlamydomonas reinhardtii*: isoform 1, 162 AA, SWP P04352.[74]
- *Arabidopsis thaliana*: plant isoform 2, 148 AA, SWP P25069.[75]
- *Arabidopsis thaliana*: plant isoform 4, 148 AA, SWP P25854.[76]
- *Arabidopsis thaliana*: plant isoform 6, 148 AA, SWP Q03509.[76]

Voltage-gated calcium channel $Ca_V\alpha1$ subunit

- *Homo sapiens*: $Ca_V1.1$ (α1S), 1873 AA, SWP Q13698.[77–79]
- *Homo sapiens*: $Ca_V1.2$ (α1C), isoform 1 (canonical, there are 35 isoforms), 2221 AA, SWP P13936.[80]
- *Homo sapiens*: $Ca_V1.2$ (α1C), isoform 20 (α1C77), 2138 AA, SWP P13936-20.[80–82]
- *Homo sapiens*: $Ca_V1.3$ (α1D), isoform Neuronal-type, 2161 AA, SWP Q01668.[83]
- *Homo sapiens*: $Ca_V1.3$ (α1D), isoform Beta-cell-type, 2181 AA, SWP Q01668-2.[84]
- *Homo sapiens*: $Ca_V1.4$ (α1F), isoform 1, 1977 AA, SWP O60840.[85]
- *Homo sapiens*: $Ca_V1.4$ (α1F), isoform 2, 1966 AA, SWP O60840-2.[85]
- *Homo sapiens*: $Ca_V2.1$ (α1A), isoform 1 (canonical, there are 7 isoforms), 2505 AA, SWP O00555.[86]
- *Oryctolagus cuniculus*: $Ca_V2.1$ (α1A), isoform BI-2 (canonical, there are 5 isoforms), 2424 AA, SWP P27884.[87]
- *Homo sapiens*: $Ca_V2.2$ (α1B), isoform α1B-1 (canonical, there are 2 isoforms), 2339 AA, SWP Q00975.[88]
- *Oryctolagus cuniculus*: $Ca_V2.2$ (α1B), 2339 AA, SWP Q05152.[89]
- *Homo sapiens*: $Ca_V2.3$ (α1E), isoform 1 (canonical, there are 3 isoforms), 2313 AA, SWP Q15878.[90]
- *Rattus norvegicus*: $Ca_V2.3$ (α1E), 2222 AA, SWP Q07652.[91]
- *Homo sapiens*: $Ca_V3.1$ (α1G), isoform 5 (canonical, there are 14 isoforms), 2377 AA, SWP O43497.[92,93]
- *Homo sapiens*: $Ca_V3.2$ (α1H), isoform 1 (canonical, there are 2 isoforms), 2353 AA, SWP O95180.[94]
- *Homo sapiens*: $Ca_V3.3$ (α1I), isoform 1 (canonical, there are 4 isoforms), 2223 AA, SWP Q9P0X4.[95,96]

PROTEIN PRODUCTION, PURIFICATION, AND MOLECULAR CHARACTERIZATION

Because they are large multicomponent membrane protein complexes (~0.5 MDa), little is known about the three-dimensional structure of complete Ca_Vs. Presently, the best data available on complete channels are low-resolution (~30 Å) electron microscopy reconstructions.[97–100] This level of structural definition reveals only the gross shape of the channel and is inadequate for developing detailed mechanistic insights. Recent crystallographic studies have yielded the first high-resolution structures of the complexes of Ca^{2+}/CaM with the C-terminal tail IQ domains of Ca_V1 and Ca_V2 subtypes (3D Structure).[23–27] These structure determination efforts have relied on either

recombinant complexes produced by coexpression in *Escherichia coli*[24,26] or *in vitro* complexes made from recombinant CaM expressed in *E. coli* and synthetic Ca_V IQ domain peptides.[23,25,27]

For coexpression production of Ca^{2+}/CaM–IQ domain complexes,[24,26] the IQ domain is expressed as a C-terminal fusion to a construct that bears in sequence a hexahistidine tag, maltose binding protein (MBP), and tobacco etch virus (TEV) protease site (termed HMT fusions for *His_6–maltose binding protein–TEV cleavage site*). HMT fusions permit the use of two, orthogonal affinity steps (metal affinity chromatography and amylose affinity chromatography) that selectively bind the hexahistidine tag and MBP, respectively. Along with the HMT fusion, untagged CaM is expressed from a second plasmid.[24,26] This approach allows the *in vivo* formation of the complex and has often been the key method for making soluble, well-behaved samples as many channel domains that interact with CaM are poorly soluble on their own.

After initial metal affinity and amylose binding affinity chromatography steps to isolate the expressed complexes, the HMT tag is removed with a specific protease, polyhistidine-tagged TEV protease.[102] Following TEV cleavage, application of the digested sample to a metal affinity purification step removes both the protease and uncleaved protein from the cleaved target material in a single step. The resulting Ca^{2+}/CaM–IQ domain complexes are then further purified using ion exchange and size-exclusion chromatography.

For complexes produced *in vitro*,[23,25,27] recombinantly expressed CaM is typically purified from the expression host using some type of hydrophobic interaction resin (ex reference 103). This method exploits the fact that Ca^{2+}/CaM binds tightly to such matrices and can be released upon the addition of a divalent chelator such as EDTA (ethylene diamine tetraacetic acid) or EGTA (ethylene glycol tetraacetic acid). Combination of purified CaM, purified synthetic peptide, and calcium ions are used to make the Ca^{2+}/CaM–IQ domain complexes that are then purified further by a gel-filtration step.[23,25,27]

X-RAY AND NMR STRUCTURE

Both calcium-free 'apo-CaM' and Ca^{2+}/CaM (Figures 2 and 3) have been the subject of numerous NMR and X-ray crystallographic studies that have investigated apo-CaM and Ca^{2+}/CaM structure alone and in complexes with a wide range of targets.[1,7,41] These studies have set the general framework for understanding how CaM acts as a calcium-sensitive switch and how it can recognize such a diverse set of protein targets. NMR studies of apo-CaM (PDB: 1CFD, 1DMO)[104,105] demonstrate that the N-lobe and C-lobe, which are tethered by a short (residue 77–80) interdomain linker, act as independent domains and have similar folds bearing two EF-hand Ca^{2+} binding motifs each (Figure 2). Upon Ca^{2+} binding, both lobes undergo a structural transformation that opens a phenylalanine- and methionine-rich hydrophobic pocket in each lobe (Figures 2 and 3). The interdomain linker is flexible in the absence of target binding[106,107] and has been seen to adopt a variety of different conformations once Ca^{2+}/CaM binds a target.[1,7,41]

The highest resolution structure of Ca^{2+}/CaM reported is at 1.0 Å (PDB: 1EXR) and is of an extended conformation in which the two lobes are separated by a long α-helix[108] (Figure 2). The crystals for these studies were grown at 4 C from a solution containing 5 mM $CaCl_2$, 50 mM sodium cacodylate (pH 5.0), and 20% methylpentanediol (MPD) equilibrated over a reservoir of 50 mM sodium cacodylate (pH 5.0), 50% MPD. They were triclinic, space group $P1$ with $a = 25.02$ Å, $b = 29.42$ Å, $c = 52.76$ Å, $\alpha = 89.54$, $\beta = 86.10$, $\gamma = 82.39$, and had one molecule per asymmetric unit. This high-resolution structure reveals

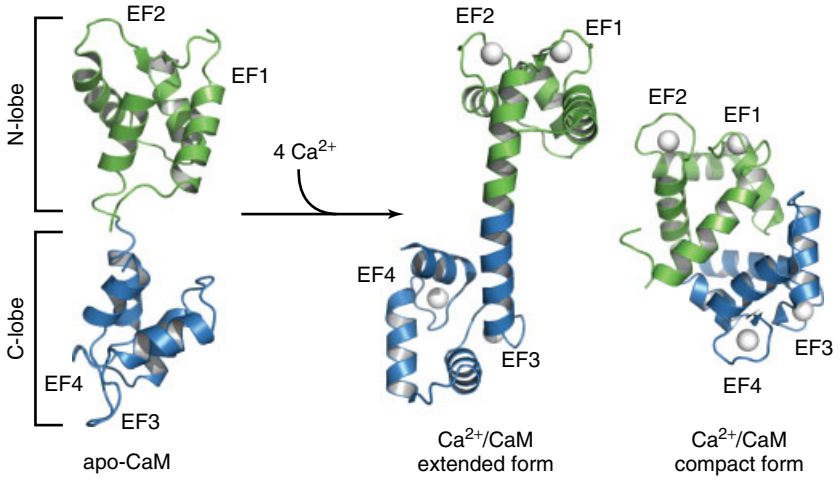

Figure 2 Structure of apo-CaM (PDB: 1CFD),[105] and Ca^{2+}/CaM in the extended (PDB: 1EXR)[108] and compact (PDB: 1PRW)[109] conformations. N-lobe and C-lobe are colored green and blue, respectively. Positions of the EF-hand domains are indicated.

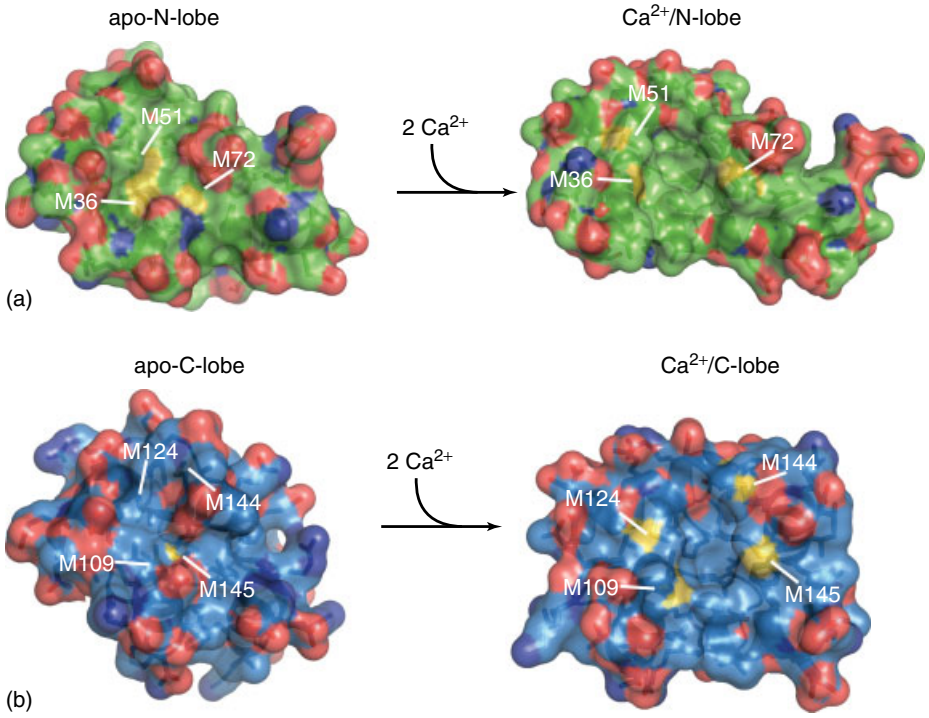

Figure 3 Ca^{2+}-dependent conformational changes expose hydrophobic pockets used for target recognition. (a and b) show views of the N-lobe (a) and C-lobe (b) hydrophobic pockets in the calcium-free (apo-state) and calcium-bound state. Structures are from (PDB: 1EXR).[108] The positions of methionine residues that are important in forming the target binding pocket are indicated.

numerous alternative conformations for residues in the binding pockets and disorder on a wide range of length scales. These unusual structural features suggest that Ca^{2+}/CaM has a large number of structural substates.[108] This high internal disorder is thought to be a crucial factor in the ability of Ca^{2+}/CaM to bind such a diverse range of targets. A crystal structure of a compact form of Ca^{2+}/CaM reported at 1.7 Å resolution (PDB: 1PRW)[109] further demonstrates the great flexibility of the interdomain linker (Figure 3). The crystals for these studies were centered monoclinic, space group $C2, a = 63.32$ Å, $b = 35.75$ Å, $c = 68.03$ Å, $\alpha = \gamma = 90.00$, $\beta = 117.19$, contained one molecule in the asymmetric unit, and were grown from 40% polyethylene glycol (PEG) 6000, 50 mM sodium acetate (pH 5.6), and 10 mM $CaCl_2$.

CaM EF-hand calcium binding architecture, ion selectivity, and ion binding affinity

The basis for Ca^{2+} recognition by CaM is the EF-hand loop[5,6] (Figure 4). This extremely well-studied calcium binding motif was first identified in the E and F helices of the calcium binding protein parvalbumin[110] and is found in many calcium binding proteins.[5,6,42] The canonical EF-hand loop is composed of a sequence of 12 residues that start with an aspartate and end with a glutamate. Six amino acid positions, denoted X, Y, Z, −X, −Y, and −Z contribute interactions to the pentagonal bipyramidal coordination of the bound calcium ion (Figure 4(a and b)). In Ca^{2+}/CaM, Ca^{2+} is hepta-coordinated by six EF-hand residues and a water molecule (Figure 4(b)). The residues at EF-hand positions X, Y, Z, and −Z use side-chain oxygen atoms to coordinate the calcium ion directly. In contrast, the −X position coordinates the Ca^{2+} ion indirectly via a water molecule and the −Y residue contributes the coordination oxygen directly from its backbone carbonyl. Consequently, the amino acid identities at the −X and −Y positions are more varied (Figure 4(a)).[5] EF hands most often occur in pairs. This arrangement allows for cooperative binding of calcium ions[5] and is the basic architecture in both CaM lobes (Figure 4).

Inside the cell, the concentration of Mg^{2+}, the element just above calcium in the IIA group of the periodic table, is ~0.5–2 mM, and presents the EF hands with a 10^2–10^4-fold excess over the Ca^{2+} concentration.[111] Thus, how EF hands achieve ion specificity has been an important question. NMR studies have demonstrated that Mg^{2+} can bind to CaM EF hands. Nevertheless, this interaction fails to cause conformational changes that alter the hydrophobic binding pocket and results in a CaM conformation that is very similar to apo-CaM.[112] Further, even though the CaM EF hands are likely to have some partial occupancy of Mg^{2+} inside the cell, the presence of up to 1 mM Mg^{2+} has no impact on EF-hand Ca^{2+} affinity.[112,113] The basis for the ion selectivity arises from the fact that Mg^{2+} is

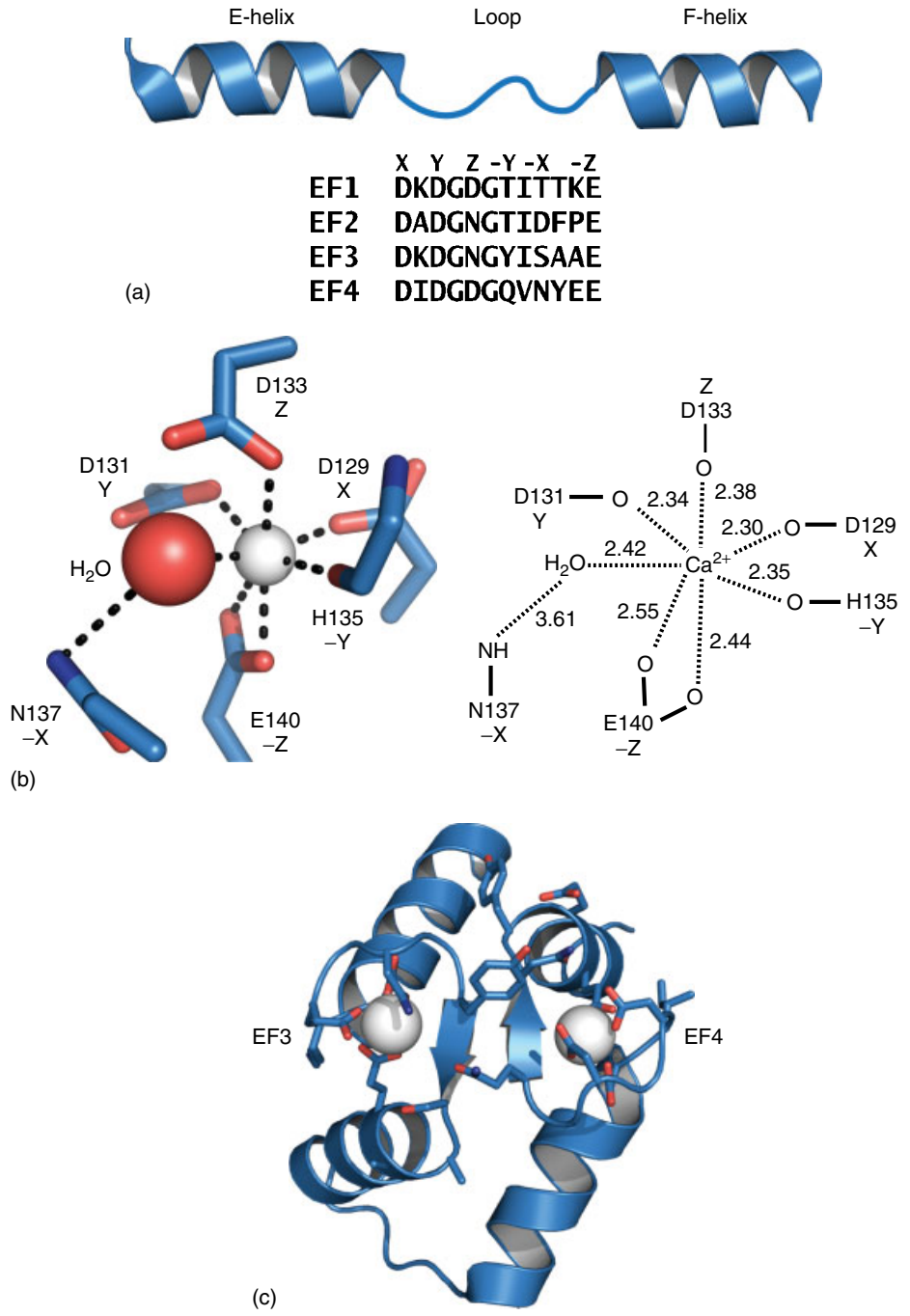

Figure 4 Ca^{2+} ion coordination by CaM EF hands. (a) EF-hand sequences for each of the four CaM EF hands from human CaM. Residues contributing to Ca^{2+} coordination are indicated. (b) View of Ca^{2+} coordination by EF4 in (PDB: 1EXR).[108] Ca^{2+} coordination distance, in angstroms, are shown schematically on the right. (c) CaM Ca^{2+}/C-lobe EF-hand pair.

much smaller, rarely uses neutral oxygen donors such as carbonyl and side-chain hydroxyls as ligands, always forms regular octahedral coordination spheres with a coordination number of six, and has a higher energetic cost of dehydration[16,111] due to its smaller ionic radius (0.65 Å and 0.99 Å for Mg^{2+} and Ca^{2+}, respectively[16]).

In the absence of targets, both CaM lobes act independently and bind calcium ions with positive cooperativity within the lobe.[114] The calcium affinities are in the range of 0.5–5 μM[113,114] with the C-lobe having ~10-fold tighter binding than N-lobe and slower binding kinetics.[115,116] Notably, both the kinetic and thermodynamic calcium binding properties can change greatly due to target engagement.[117–125] In particular, CaM binding to Ca_V1 and Ca_V2 IQ domains has been reported to increase the apparent Ca^{2+} affinity by ~20–100-fold.[23,126] Thus,

there is a clear interplay between the target and CaM that can tune the calcium response of specific complexes.

Ca^{2+}/CaM – Ca_V1 and Ca_V2 IQ domain complexes

The IQ motif, (I/L/V)QXXXRXXXX(R/K), named for the isoleucine–glutamine (IQ) pair, is a Ca^{2+}/CaM and apo-CaM binding motif found in diverse proteins including molecular motors, voltage-gated calcium channels, voltage-gated sodium channels, and phosphatases.[127–129] All Ca_V1s and Ca_V2s have an IQ motif located in the C-terminal cytoplasmic tail ~150–180 residues C-terminal to the last transmembrane segment (IVS6) (Figure 1). This site functions as the principal Ca^{2+}/CaM binding site and has been shown to be crucial for both CDI and CDF in both Ca_V1 and Ca_V2s.[24,26,27,34,35,37,130–132]

To simplify comparisons, and because the Ca_V IQ sequences have different numbering schemes depending on the organism of origin and particular splice variant used, the IQ domain positions are designated by their relative position in the sequence with respect to the central isoleucine, Ile(0), with negative and positive numbers signifying the position of each residue N-terminal or C-terminal with reference to Ile(0), respectively (Figure 1(c)).

Ca_V1 IQ complexes

The first structures of Ca^{2+}/CaM–Ca_V IQ domain complexes were reported using the IQ domains of the L-type channel $Ca_V1.2$[24,25] (Figure 5). These structures were not only the first description of Ca^{2+}/CaM bound to a Ca_V IQ domain but were also the first description of a Ca^{2+}/CaM–IQ domain complex from any source. The Ca^{2+}/CaM–$Ca_V1.2$ IQ domain structures (PDB: 2BE6, 2F3Y)[24,25] showed that Ca^{2+}/CaM wraps around an α-helix formed by the IQ domain (Figure 5). For 2BE6, crystals of the complex were monoclinic, space group $P2_1$, $a = 84.73$ Å, $b = 37.24$ Å, $c = 86.86$ Å, $\alpha = \gamma = 90.00$, $\beta = 97.77$, contained three complexes in the asymmetric unit, and were grown from 20–30% PEG 3350, 0.1 M Bis–Tris (pH 6.5). The crystals used in 2F3Y were centered monoclinic, space group $C2$, $a = 86.20$ Å, $b = 30.96$ Å, $c = 63.94$ Å, $\alpha = \gamma = 90.00$, $\beta = 114.54$, contained one complex in the asymmetric unit, and were

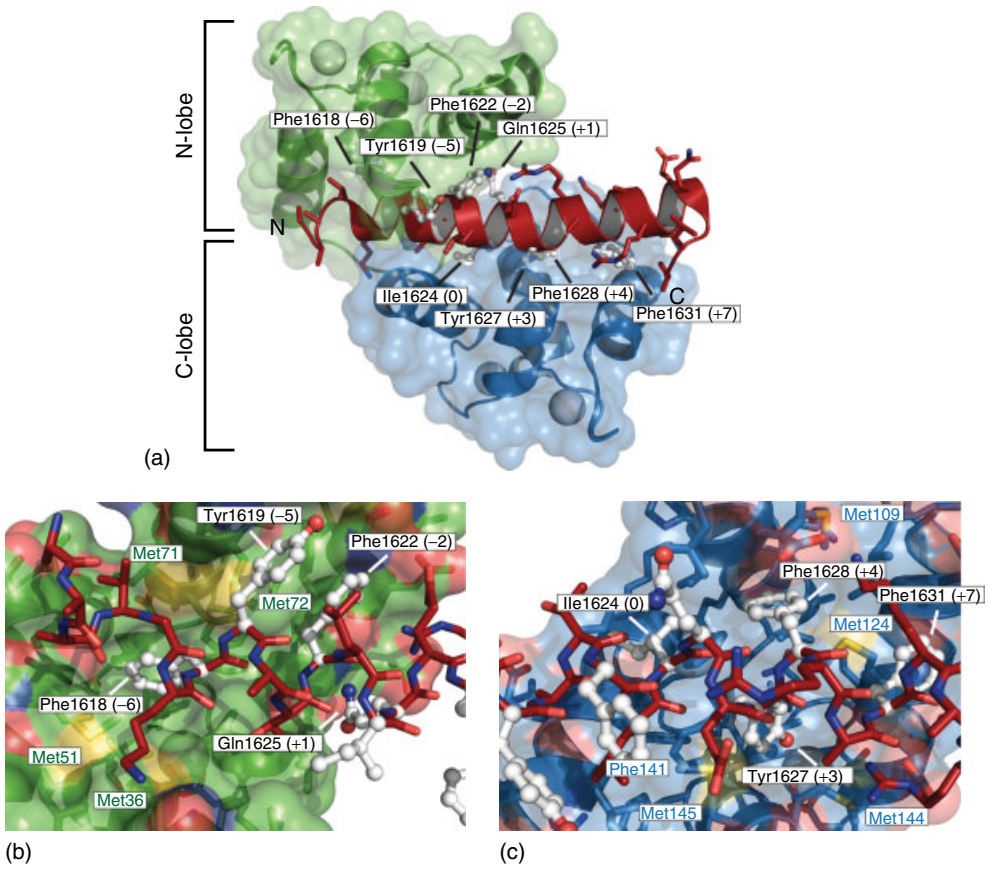

Figure 5 (a) Structure of the Ca^{2+}/CaM–$Ca_V1.2$ IQ peptide complex (PDB: 2BE6).[24] Ca^{2+}/N-lobe and Ca^{2+}/C-lobe are shown in green and blue, respectively. $Ca_V1.2$ IQ domain is shown in firebrick and the aromatic anchor positions are white and shown in ball-and-stick representation. The 'IQ' positions are labeled. (b) Close-up view of the Ca^{2+}/N-lobe-$Ca_V1.2$ IQ domain interactions. (c) Close-up view of the Ca^{2+}/C-lobe–$Ca_V1.2$ IQ domain interactions.

grown from 32% PEG 4000, 50 mM $MgCl_2$, 50 mM Tris (pH 8.3).

In the 2BE6 structures,[24] which have longer IQ domains, the IQ helix has a ~10 bend, centered on Ile1624(0). The structures uncovered two key, unanticipated features. First, the complex revealed a parallel binding mode in which Ca^{2+}/N-lobe was bound to the N-terminal portion of the IQ helix, whereas Ca^{2+}/C-lobe was bound to the C-terminal end. Previously, only one other Ca^{2+}/CaM-α-helical peptide complex had shown this type of binding orientation, that of the Ca^{2+}/CaM-dependent kinase kinase.[133,134] All other examples of Ca^{2+}/CaM–peptide complexes adopted an antiparallel arrangement with respect to Ca^{2+}/CaM and the bound helical peptide. Second, the structures revealed that each Ca^{2+}/CaM lobe interacts with three principle aromatic residues, termed *aromatic anchors* arranged on opposite faces of the IQ helix (Figures 1(c) and 5).

In the Ca^{2+}/CaM–$Ca_V1.2$ IQ domain complex, Phe1618(−6), Tyr1619(−5), and Phe1622(−2) form the aromatic anchors that interact with Ca^{2+}/N-lobe (Figure 5(b)). In 2BE6, two conformations of the Ca^{2+}/N-lobe were observed (denoted, Chain A and Chain C). These use the same set of aromatic anchors but tilt and shift the position of Ca^{2+}/N-lobe to make a slightly more compact structure in the one from Chain C. Tyr1627(+3), Phe1628(+4), and Phe1631(+7) form the aromatic anchors that interact with Ca^{2+}/C-lobe (Figure 5(c)). From the IQ hallmark residues, Ile1624(0) is completely buried by interactions with Ca^{2+}/C-lobe and Gln1625(+1) interacts with both Ca^{2+}/N-lobe and Ca^{2+}/C-lobe. The key contacts are similar in both PDB: 2BE6, 2F3Y. Additionally, Fallon *et al.*[25] determined the structure of an IQ domain mutant (PDB: 2F3Z) that incorporated the IQ → AA change at positions 0 and +1. These crystals were isomorphic to 2F3Y and grown in the same crystallization conditions. In $Ca_V1.2$, the IQ → AA double mutant eliminates CDI and causes strong CDF,[135] but does not alter the ability of Ca^{2+}/CaM to bind the IQ domain.[135,136] The structure of this mutant complex is essentially identical to the wild-type complex (root mean square deviation for Cα atoms, $r.m.s.d._C = 0.530$).

$Ca_V1.1$ channels are unusual. Their principle role is to act in skeletal muscle as the voltage-sensing subunit for the intracellular ryanodyne receptor.[16] This action requires a physical link between $Ca_V1.1$ and the ryanodyne receptor but does not require calcium permeation through $Ca_V1.1$.[137–141] Nevertheless, $Ca_V1.1$ subunits do have some form of CDI[142] and an IQ domain that is capable of binding Ca^{2+}/CaM.[23,143] The 1.94-Å resolution structure of Ca^{2+}/CaM–$Ca_V1.1$ IQ domain complex[23] (PDB: 2VAY) reveals a parallel binding conformation that is very similar to that observed in the $Ca_V1.2$ complexes (Table 2). These crystals were centered monoclinic, space group $C2$, $a = 84.92$ Å, $b = 34.67$ Å, $c = 62.98$ Å, $\alpha = \gamma = 90.00$, $\beta = 113.59$, contained one complex in the asymmetric unit, and were grown in 32% PEG 3500, 50 mM $MgCl_2$, 50 mM Tris. This crystal habit and growth conditions are very similar to those of 2F3Y and 2F3Z. Of the four residues that are not conserved between $Ca_V1.1$ and $Ca_V1.2$ (positions +3, +8, +11, and +13) (Figure 1(c)), only the anchor position residue $Ca_V1.1$ His1532(+3) and $Ca_V1.2$ Tyr1627(+3) make substantial contacts with Ca^{2+}/CaM. Structural analysis shows that $Ca_V1.1$ His1532 (+3) occupies the same Ca^{2+}/C-lobe binding pocket as $Ca_V1.2$ Tyr1627(+3). This change requires only a minor rearrangement of the side chains that line the pocket.[23] Introduction of the Y → H(+3) change into the $Ca_V1.2$ IQ domain is sufficient to reduce Ca^{2+}/CaM binding. Simultaneous introduction of Y(+3) → H(+3) and K(+8) → M(+8) into $Ca_V1.2$ eliminates CDI.[143]

Ca_V2 IQ complexes

The determination of Ca^{2+}/CaM–Ca_V IQ domain complexes from $Ca_V2.1$, $Ca_V2.2$, and $Ca_V2.3$ at 2.6, 2.35, and 2.30 Å resolution (PDB: 3DVM, 3DVE, and 3DVK), respectively, revealed that unlike the $Ca_V1.2$ and $Ca_V1.1$ Ca^{2+}/CaM-IQ domain complexes, all three Ca_V2 IQ domain complexes are antiparallel (Figure 6). The $Ca_V2.1$ complex crystals (3DVM) were primitive hexagonal, space group $P6_122$, $a = b = 44.0$ Å $c = 337.9$ Å, $\alpha = \beta = 90.00$, $\gamma = 120.00$, contained one complex in the asymmetric unit and were grown in 25% PEG 3350, 0.1 M Bis–Tris (pH 6.5). Crystals of the $Ca_V2.2$ and $Ca_v2.3$ complexes (3DVE and 3DVK) were primitive hexagonal, space group $P6_122$, had unit-cell dimensions of $a = b = 44.3$ Å, $c = 344.7$ Å, $\alpha = \beta = 90.00$, $\gamma = 120.00$, and $a = b = 44.3$ Å, $c = 337.9$ Å, $\alpha = \beta = 90.00$, $\gamma = 120.00$, respectively. Each contained one complex in the asymmetric unit and were grown from 25 to 30% PEG 2000 monomethylether (MME), 0.1 M Bis–Tris (pH 6.5).

Rather than just a simple exchange of binding positions, the Ca_V2 antiparallel complexes also show a translation of Ca^{2+}/CaM toward the N-terminal end of the IQ helix (Figure 7). This shift is consistent with the loss of the aromatic anchor at the +7 position, which is a small hydrophilic residue in all of the Ca_V2 IQ domains (Figure 1(c) and 7). As a consequence of the more N-terminally located binding of Ca^{2+}/CaM, Ca^{2+}/N-lobe is anchored by four main residues: methionine (−1), isoleucine (0), and the aromatics at positions (+3) and (+5). Ca^{2+}/C-lobe, which is bound to the N-terminal end of the IQ helix, is anchored by only two major positions, (−6) and (−2).

While the $Ca_V2.1$ and $Ca_V2.3$ complexes are essentially identical ($r.m.s.d._C = 0.598$), the $Ca_V2.2$ complex displayed some structural differences ($r.m.s.d._C = 2.02$ for superposition using $Ca_V2.2$ and $Ca_V2.3$ Ca^{2+}/N-lobes and IQ domains), namely, a slightly altered IQ helix pose and a relative displacement of the Ca^{2+}/C-lobe toward the center of the IQ helix. These differences

Table 2 Structure comparison of Ca^{2+}/CaM-IQ domain complexes

Native channel		L-type					Non-L-type					
							P/Q-type		N-type		R-type	
	Pore-forming $Ca_V\alpha_1$ subunit	α_{1S}, $Ca_V1.1$, 2VAY	α_{1C}, $Ca_V1.2$, 2BE6, Chain A	α_{1C}, $Ca_V1.2$, 2BE6, Chain C	α_{1C}, $Ca_V1.2$, 2F3Y	α_{1C}, $Ca_V1.2$, 2F3Z, IQ→AA	α_{1A}, $Ca_V2.1$, 3DVM,	α_{1A}, $Ca_V2.1$, 3BXK	α_{1B}, $Ca_V2.2$, 3DVE,	α_{1B}, $Ca_V2.2$, 3DVJ,	α_{1E}, $Ca_V2.3$, 3DVK,	α_{1E}, $Ca_V2.3$, 3BXL
L-type	α_{1S}, $Ca_V1.1$, 2VAY[23]	–	–	–	–	–	–	–	–	–	–	–
	α_{1C}, $Ca_V1.2$, 2BE6, Chain A[24]	**0.831**	–	–	–	–	–	–	–	–	–	–
	α_{1C}, $Ca_V1.2$, 2BE6, Chain C[24]	**1.140**	**0.738**	–	–	–	–	–	–	–	–	–
	α_{1C}, $Ca_V1.2$, 2F3Y[25]	**0.684**	**0.848**	**1.061**	–	–	–	–	–	–	–	–
	α_{1C}, $Ca_V1.2$, 2F3Z, IQ → AA[25]	**0.847**	**0.821**	**1.154**	**0.602**	–	–	–	–	–	–	–
Non-L-type P/Q-type	α_{1A}, $Ca_V2.1$, 3DVM,[26]	1.917	2.037	1.990	1.869	1.885	–	–	–	–	–	–
	α_{1A}, $Ca_V2.1$, 3BXK[27]	**1.478**	**0.868**	**0.643**	**1.319**	**1.507**	2.356	–	–	–	–	–
Non-L-type N-type	α_{1B}, $Ca_V2.2$, 3DVE,[26]	2.128	2.164	2.077	2.156	2.182	1.514	2.405	–	–	–	–
	α_{1B}, $Ca_V2.2$, 3DVJ, HM → TV[26]	2.141	2.125	2.221	2.177	2.188	1.402	2.451	0.447	–	–	–
Non-L-type R-type	α_{1E}, $Ca_V2.3$, 3DVK,[26]	**2.141**	**1.983**	**1.923**	**1.779**	**1.810**	0.598	2.285	1.699	1.576	–	–
	α_{1E}, $Ca_V2.3$, 3BXL,[27]	**1.836**	**1.309**	**0.938**	**1.311**	**1.476**	2.136	**0.621**	2.109	2.175	2.069	–

Black numbers indicate superposition based on Ca^{2+}/C-lobe and IQ domain. Green numbers indicate superposition based on Ca^{2+}/N-lobe and IQ domain. Blue numbers indicate superposition based on Ca^{2+}/C-lobe-IQ domain with Ca^{2+}/N-lobe-IQ domain. In all cases, the lobe used for superposition is the one bound to the C-terminal site of the IQ domain. All values are for r.m.s.d.$_C$.

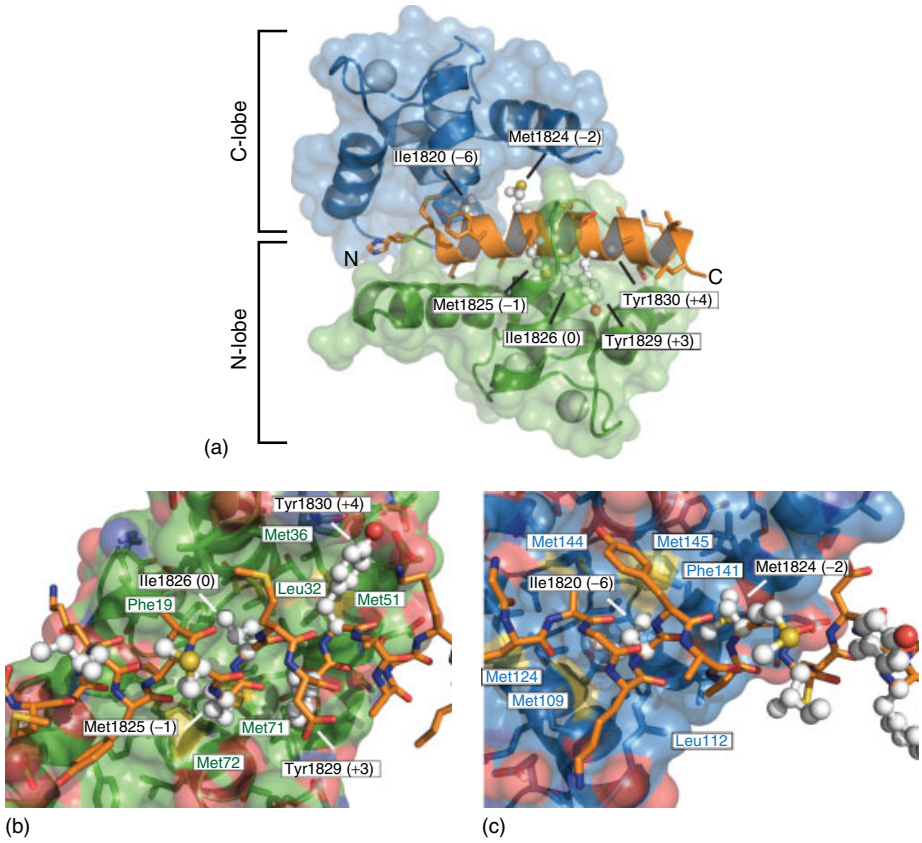

Figure 6 (a) Structure of Ca^{2+}/CaM–Ca_V2 IQ peptide complex (PDB: 3DVK).[26] Ca^{2+}/N-lobe and Ca^{2+}/C-lobe are shown in green and blue, respectively. $Ca_V2.3$ IQ domain is shown in orange and the aromatic anchor positions are white and shown in ball-and-stick representation. (b) Close-up view of the Ca^{2+}/N-lobe-$Ca_V2.3$ IQ domain interactions. (c) Close-up view of the Ca^{2+}/C-lobe-$Ca_V2.3$ IQ domain interactions.

cause less burial of Met1862 (−1), more Ca^{2+}/N-lobe interactions to Phe1864(+1) than made in $Ca_V2.1$ and $Ca_V2.3$ to Met1972/1827(+1), and a more central position of Ile1863(0) in the $Ca_V2.2$ complex. In all structures, the Tyr(+4) side-chain hydroxyl makes a water-mediated hydrogen bond with the Ca^{2+}/N-lobe.

In addition to the above structures, complexes of Ca^{2+}/CaM with $Ca_V2.1$ and $Ca_V2.3$ IQ peptides shorter than those described above (Table 1) were also reported (PDB: 3BXK and 3BXL, respectively).[27] The $Ca_V2.1$ complex crystals were centered monoclinic, space group C2, had unit-cell dimensions of $a = 80.65$ Å, $b = 80.43$ Å, $c = 63.84$ Å, $\alpha = \gamma = 90.00$, $\beta = 97.56$, contained two complexes in the asymmetric unit, and were grown from 2.3 M ammonium sulfate, 0.15 M sodium tartrate, and 0.05 M sodium citrate (pH 5.5). The $Ca_V2.3$ complex crystals were centered tetragonal, space group $I4_122$, had unit-cell dimensions of $a = b = 124.61$ Å, $c = 74.02$ Å, $\alpha = \beta = \gamma = 90.00$, contained one complex in the asymmetric unit, and were grown from 2.1 M ammonium sulfate and 0.05 M sodium citrate (pH 5.0).

Strikingly, the structures of these complexes are very similar to the parallel $Ca_V1.2$ complex using the short

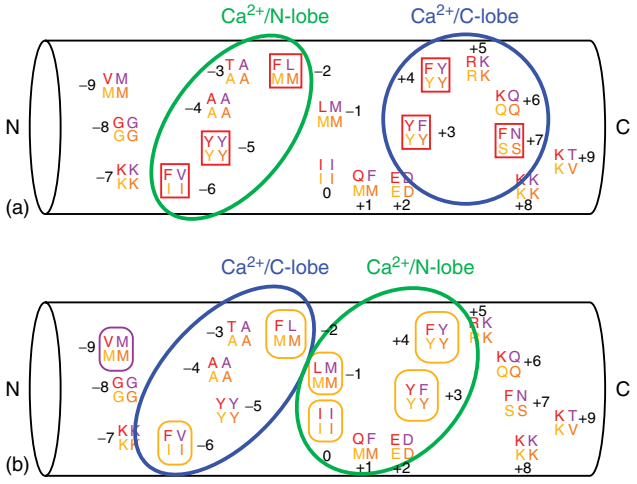

Figure 7 Comparisons of the anchor positions used by the individual Ca^{2+}/CaM lobes in the parallel $Ca_V1.2$ complex (a) and antiparallel Ca_V2 complexes (b). Ca^{2+}/N-lobe and Ca^{2+}/C-lobe are shown in green and blue, respectively. Sequences from $Ca_V1.2$, $Ca_V2.1$, $Ca_V2.2$, and $Ca_V2.3$ are shown in red, yellow, purple, and orange, respectively. Red boxes indicate the aromatic anchors in the $Ca_V1.2$ complex. Yellow ovals indicate the anchor positions used in the Ca_V2 complexes. Purple oval shows an additional contact to Ca^{2+}/C-lobe in the $Ca_V2.2$ complex.

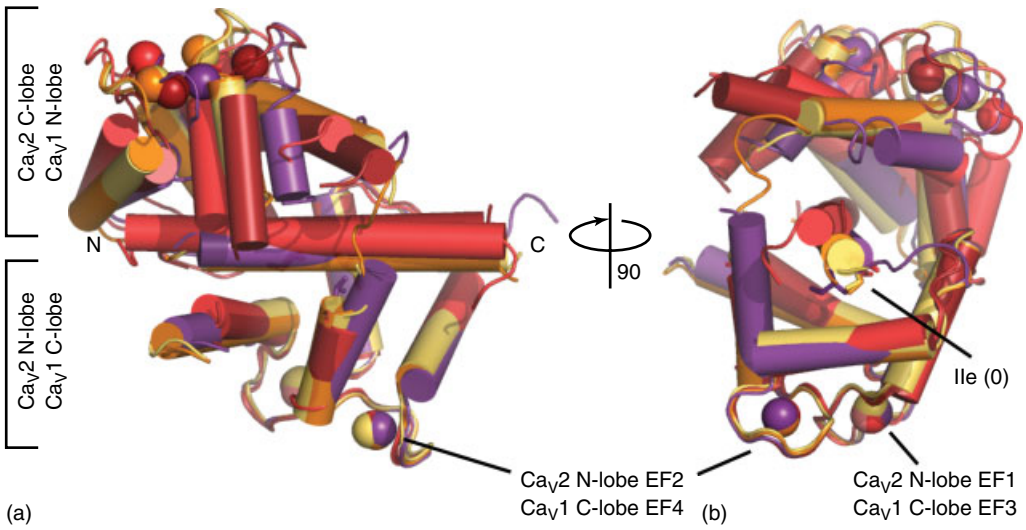

Figure 8 Comparison of the Ca^{2+}/CaM–$Ca_V1.2$ and Ca^{2+}/CaM–Ca_V2 parallel and antiparallel structures using superposition of Ca^{2+}/C-lobe–$Ca_V1.2$ and Ca^{2+}/N-lobe–Ca_V2s. Structures are colored as follows: Ca^{2+}/CaM–$Ca_V1.2$ IQ domain (firebrick), Ca^{2+}/CaM–$Ca_V2.1$ IQ domain (yellow), Ca^{2+}/CaM–$Ca_V2.2$ IQ domain (purple), Ca^{2+}/CaM–$Ca_V2.3$ IQ domain (orange). (a) Side view. All IQ helices have the same orientation. (b) Axial view from the C-terminus of the IQ domain.

peptide reported by Fallon *et al.*[25] The ability of Ca^{2+}/CaM to bind similar peptide sequences in opposite orientations is striking. It should be noted, however, that the shorter peptides lack four residues that contribute to interactions with the C-lobe in the antiparallel complexes, particularly the residue at (−9), and adoption of the antiparallel pose on the short peptide would place the positively charged IQ peptide N-terminus near the C-lobe. Notably, the peptide length is not an issue for $Ca_V1.2$ binding as the 2BE6 structures contain a peptide that begins at position (−12).

Comparison of parallel and antiparallel binding modes

In both the parallel Ca_V1- and antiparallel Ca_V2–Ca^{2+}/CaM IQ domain complexes, each Ca^{2+}/CaM lobe interacts with an extensive network of residues from the IQ helices. One common element in the Ca_V1 and Ca_V2 complexes is that the occupant of the N-terminal binding site, Ca^{2+}/N-lobe for Ca_V1s and Ca^{2+}/C-lobe for Ca_V2s, buries much less surface area than the occupant of the C-terminal binding site (Ca^{2+}/N-lobe vs Ca^{2+}/C-lobe: $Ca_V1.1$ 1209 $Å^2$, 1630 $Å^2$; $Ca_V1.2$ 1450 $Å^2$, 1819 $Å^2$; $Ca_V2.1$ 1652 $Å^2$, 921 $Å^2$; $Ca_V2.2$ 2026 $Å^2$, 1224 $Å^2$; $Ca_V2.3$ 1673 $Å^2$, 950 $Å^2$; respectively). Aside from the helix direction, the constellation of anchor points has major differences (Figure 7). In all antiparallel Ca_V2 complexes, Ca^{2+}/CaM binds further toward the IQ helix N-terminal end, a change that is consistent with the lack of an aromatic residue at (+7), a position that is a key anchor for Ca^{2+}/C-lobe in the Ca_V1 complexes. Four aromatic anchor positions used by the $Ca_V1.2$ IQ α-helix to bind Ca^{2+}/CaM, positions (−6), (−2), (+3) and (+4), are also used as anchors in the Ca^{2+}/CaM–Ca_V2 IQ helix complexes. Ca^{2+}/C-lobe binds two of these, (−6) and (−2), neither of which are aromatic residues in Ca_V2s but that retain nonpolar character, whereas Ca^{2+}/N-lobe uses the two aromatics at (+3) and (+4). The more N-terminal location of Ca^{2+}/N-lobes in the Ca_V2 complexes results in the (−1) and (0) positions occupying a very central position in the Ca^{2+}/N-lobe binding site (Figures 6(a) and 7(b)).

Ca^{2+}/N-lobe and Ca^{2+}/C-lobe share a high degree of structural similarity.[43] This is evident if one superposes the Ca^{2+}/C-lobe of the $Ca_V1.2$ parallel complex onto Ca^{2+}/N-lobe of the antiparallel Ca_V2 complexes (Figure 8). This superposition preserves the IQ helix direction and shows that Ca^{2+}/CaM wraps around the IQ helix by using different amounts of lobe separation along the helix. Comparison of all of the structures is shown in Table 2. The largest degree of separation is found in the $Ca_V1.2$ complex. The relative position of the N-terminally located lobe with respect to the IQ helix axis is delimited by the two conformations seen for Ca^{2+}/N-lobe in the $Ca_V1.2$ structure (Figure 8(b)).

FUNCTIONAL ASPECTS

The processes of CDI and CDF provide opposing ways for Ca_Vs to autoregulate activity.[28,32,33] Both depend on the interaction of Ca^{2+}/CaM with the IQ domain. Elegant experiments using CaM mutants impaired in calcium binding at specific lobes have demonstrated that the individual lobes cause CDI in a manner that is exchanged between Ca_V1 and Ca_V2 isoforms. In $Ca_V1.2$, the C-lobe governs CDI[37] (Figure 9(a)), whereas in

$Ca_V2.1$[34,35] (Figure 10(a)), $Ca_V2.2$,[36] and $Ca_V2.3$[36] the N-lobe governs CDI. Further, the C-lobe has been shown to control $Ca_V2.1$ CDF.[34,35] Functional analysis based on the $Ca_V1.2$ structure deepened the mystery further. Elimination of the interactions between the N-lobe anchors Phe1618(−6), Tyr1619(−5), and Phe1622(−2) by a triple alanine mutation (TripleA), abolished $Ca_V1.2$ CDF and Ca^{2+}/N-lobe binding[24] (Figure 9(b)). This result suggests a complete inversion of lobe-specific roles between $Ca_V1.2$ and $Ca_V2.1$ (Figure 11(a)).

The high level of sequence similarity among the Ca_V1 and Ca_V2 IQ domains (Figure 1(c)) and the inversion of lobe-specific functions (Figure 11(a)), pushed the desire to understand how the same molecule, Ca^{2+}/CaM, could affect different processes using different lobes and yet interact with a highly conserved portion of the pore-forming subunit. The antiparallel orientation revealed in the Ca^{2+}/CaM complexes with the longest Ca_V2 IQ domains, together with the observation that structure-based alanine mutations that eliminate the binding of the C-lobe to the IQ domain also greatly reduce CDF[26] (Figure 10(b)) indicates a clear structural basis for the swap of lobe-specific roles. These data suggest that the Ca_V1 and Ca_V2 IQ domains contain dedicated CDF binding sites and that the occupant of those sites is exchanged between Ca_V1 and Ca_V2 isoforms (Figure 11). The observed inversion of structural polarity provides an attractive explanation for the inversion of lobe-specific roles (Figure 11(b)) (however, see reference 27 for alternative scenarios). The observation that the occupant of the N-terminal site in both Ca_V1 and Ca_V2 IQ domains makes fewer contacts and binds more weakly, suggests that these physical properties are also key to the CDF mechanism.

Despite the advances in understanding the structural interactions of Ca^{2+}/CaM with Ca_V IQ domains, the view remains limited. It is unclear how the channel senses the conformation changes on the IQ domain and how these are linked to changes in the behavior of the channel pore. Further, apo-CaM binds the Ca_V C-terminal tails of both L-type and non-L-type Ca_Vs[31,37,130,144–147] and is thought to be essential for the ability of Ca_Vs to decode different types of calcium signals[148]; however, the exact binding site and details of the interactions remain controversial. At least three-candidate Ca_V C-terminal tail regions have been proposed: the IQ domain,[136,146,149] and two regions in the 'pre-IQ' region that are termed the *A-peptide*[149] and *C-peptide* regions.[136,145,149,150]

As there is a substantial amount of the Ca_V mass in the cytoplasm, ~150 kDa,[28] other elements from the intracellular regions of the channel are likely to have some role in both CDI and CDF. Functional data point toward potential roles for interaction of the Ca^{2+}/CaM IQ domain with the putative EF hand proximal to transmembrane segment IV6,[27,151] elements in the N-terminal[148,152,153] and the C-terminal $Ca_V\alpha_1$ cytoplasmic domains,[154–157] and the $Ca_V\beta$ subunit.[149,158,159] Additionally, the large, dodecameric protein kinase, CaMKII has been shown to be a key element in both $Ca_V1.2$[160–164] and $Ca_V2.1$[165] CDF. Exactly how this large complex engages the channel remains unknown.

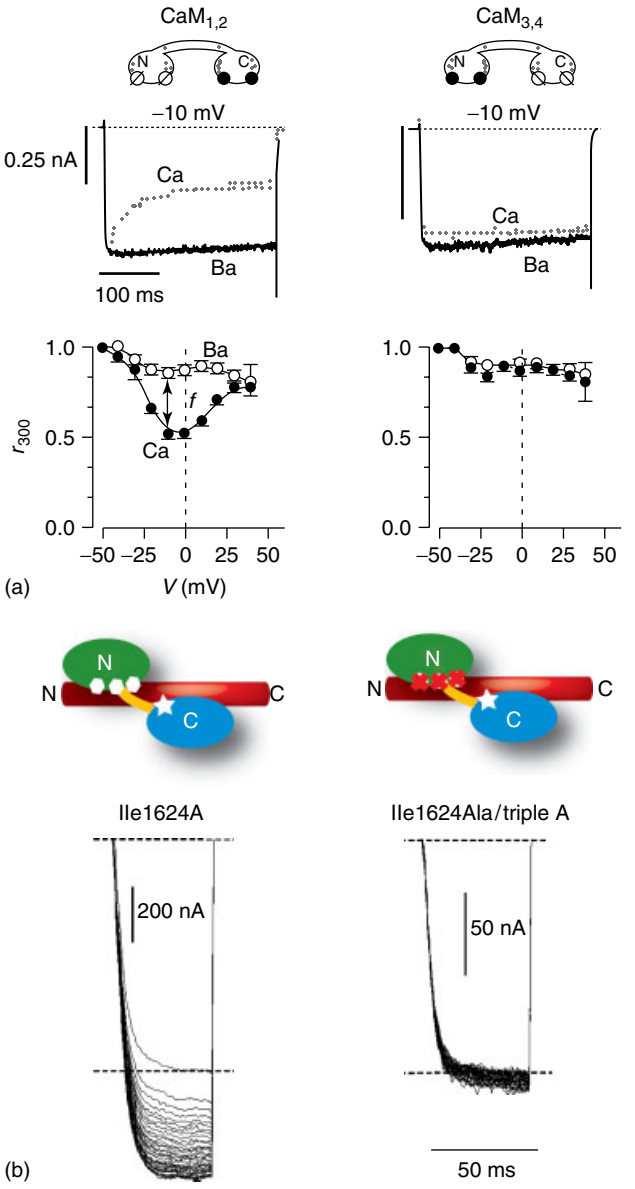

Figure 9 Calmodulin modulation of $Ca_V1.2$ (a) Lobe-specific CaM mutants defective in Ca^{2+} binding, $CaM_{1,2}$ (defective N-lobe), and $CaM_{3,4}$ (defective C-lobe) demonstrate the importance of C-lobe for $Ca_V1.2$ CDI. Top shows response of $Ca_V1.2$ to a depolarization to −10 mV when Ca^{2+} (gray) or Ba^{2+} (black) is the charge carrier. Bottom shows the residual current at 300 ms for both charge carriers (from reference 37). (b) Elimination of Ca^{2+}/N-lobe aromatic anchors abolishes $Ca_V1.2$ CDF. Experiments show the response of $Ca_V1.2$ to a 3-Hz pulse train (50 ms steps to +20 mV from a holding potential of −90 mV) and are done in the background of the I1624A mutant that unmasks CDF. Cartoons show the positions of the Ca^{2+}/N-lobe aromatic anchors (hexagons) and I1624A (star) (Reproduced with permission from Ref. 24. © Nature).

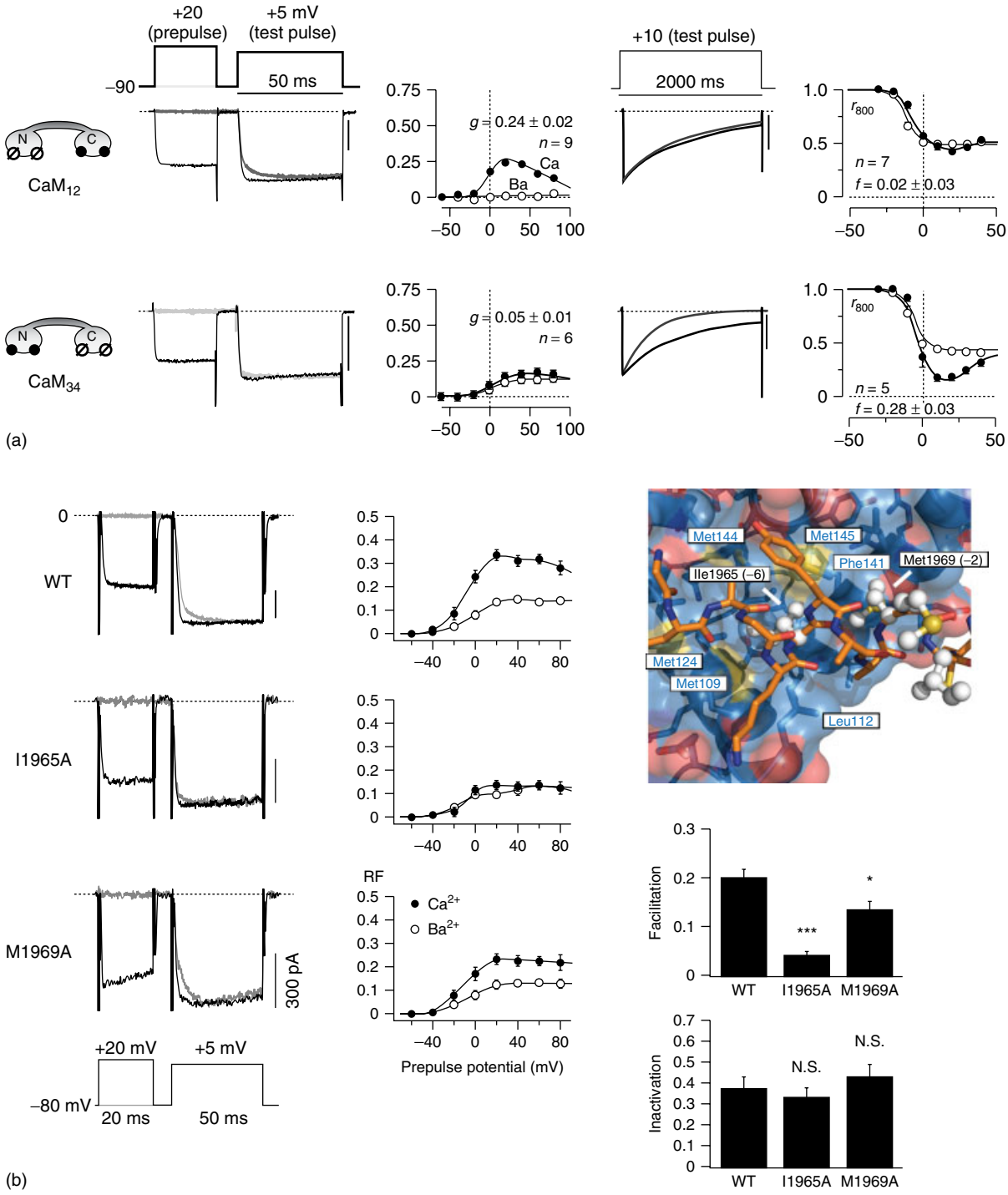

Figure 10 Calmodulin modulation of $Ca_V1.2$. (a) Lobe-specific CaM mutants defective in Ca^{2+} binding, CaM_{12} (defective N-lobe), and CaM_{34} (defective C-lobe) demonstrate the importance of N-lobe for $Ca_V2.1$ CDI and C-lobe for $Ca_V2.1$ CDF. Left shows response of $Ca_V2.1$ to a depolarization to +5 mV following a prepulse to +20 mV and a measure of relative facilitation when Ca^{2+} (gray) or Ba^{2+} (black) is the charge carrier. Right shows response to a +10 mV pulse and inactivation at 800 ms for both charge carriers (from reference 34). (b) Elimination of Ca^{2+}/C-lobe anchors demonstrates importance for $Ca_V2.1$ CDF. Left shows response of $Ca_V2.1$ and I1965(−6) and M1969(−2) anchor mutants to protocols similar to (a). Right shows positions of (−6) and (−2) anchors and the alanine mutant effects on facilitation and inactivation (Reproduced with permission from Ref. 26. © Elsevier).

The acquisition of high-resolution structural views of the interactions of Ca^{2+}/CaM with various Ca_V1 and Ca_V2 IQ domains has provided significant insight into the complex mechanisms that control Ca_V activity-dependent modulation. Nevertheless, the IQ domain is too far from the pore-lining segments in primary sequence to postulate

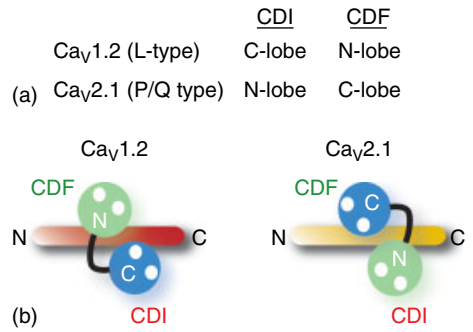

Figure 11 Functional and structural correlates of Ca^{2+}/CaM interactions with Ca_V1 and Ca_V2 IQ domains. (a) Lobe-specific roles in $Ca_V1.2$ and $Ca_V2.1$ CDI and CDF. (b) Diagrams of the orientations of Ca^{2+}/CaM on the Ca_V1 and Ca_V2 IQ domains and the roles of the individual lobes.

a simple model for how the Ca^{2+}/CaM IQ domain complexes mediate CDI and CDF. Thus, defining the exact arrangement of the channel intracellular components and the state dependence of interactions remains an important challenge for future work.

REFERENCES

1. M Ikura and JB Ames, *Proc Natl Acad Sci U S A*, **103**, 1159–64 (2006). DOI: 0508640103 [pii] 10.1073/pnas.0508640103.
2. RD Burgoyne, *Nat Rev Neurosci*, **8**, 182–93 (2007). DOI: nrn2093 [pii] 10.1038/nrn2093.
3. TN Tsalkova and PL Privalov, *J Mol Biol*, **181**, 533–44 (1985). DOI: 0022–2836(85)90425-5 [pii].
4. L Masino, SR Martin and PM Bayley, *Protein Sci*, **9**, 1519–29 (2000). DOI: 10.1110/ ps.9.8.1519.
5. JL Gifford, MP Walsh and HJ Vogel, *Biochem J*, **405**, 199–221 (2007). DOI: BJ20070255 [pii] 10.1042/BJ20070255.
6. Z Grabarek, *J Mol Biol*, **359**, 509–25 (2006). DOI: S0022-2836(06)00447-5 [pii] 10.1016/j.jmb.2006.03.066.
7. KP Hoeflich and M Ikura, *Cell*, **108**, 739–42 (2002).
8. AP Yamniuk and HJ Vogel, *Mol Biotechnol*, **27**, 33–57 (2004). DOI: MB:27:1:33 [pii] 10.1385/MB:27:1:33.
9. KL Yap, J Kim, K Truong, M Sherman, T Yuan and M Ikura, *J Struct Funct Genomics*, **1**, 8–14 (2000).
10. Y Saimi and C Kung, *Annu Rev Physiol*, **64**, 289–311 (2002).
11. WA Catterall, *Annu Rev Cell Dev Biol*, **16**, 521–55 (2000).
12. EA Ertel, KP Campbell, MM Harpold, F Hofmann, Y Mori, E Perez-Reyes, A Schwartz, TP Snutch, T Tanabe, L Birnbaumer, RW Tsien and WA Catterall, *Neuron*, **25**, 533–35 (2000). DOI: S0896-6273(00)81057-0 [pii].
13. WA Catterall, E Perez-Reyes, TP Snutch and J Striessnig, *Pharmacol Rev*, **57**, 411–25 (2005). DOI: 57/4/411 [pii] 10.1124/pr.57.4.5.
14. MC Jeziorski, RM Greenberg and PA Anderson, *J Exp Biol*, **203**, 841–56 (2000).
15. Y Okamura, H Izumi-Nakaseko, K Nakajo, Y Ohtsuka and T Ebihara, *Neurosignals*, **12**, 142–58 (2003). DOI: 10.1159/000072161 NSG2003012003142 [pii].
16. B Hille, *Ion Channels of Excitable Membranes*, 3rd edn, Sinauer Associates, Inc., Sunderland, MA (2001).
17. FH Yu, V Yarov-Yarovoy, GA Gutman and WA Catterall, *Pharmacol Rev*, **57**, 387–95 (2005).
18. K Talavera and B Nilius, *Cell Calcium*, **40**, 97–114 (2006). DOI: S0143-4160(06)00080-7 [pii] 10.1016/j.ceca.2006.04.013.
19. MC Iftinca and GW Zamponi, *Trends Pharmacol Sci*, **30**, 32–40 (2009). DOI: S0165-6147(08)00242-3 [pii] 10.1016/j.tips.2008.10.004.
20. I Calin-Jageman and A Lee, *J Neurochem*, **105**, 573–83 (2008). DOI: JNC5286 [pii] 10.1111/j.1471–4159.2008.05286.x.
21. HW Tedford and GW Zamponi, *Pharmacol Rev*, **58**, 837–62 (2006).
22. WA Catterall and AP Few, *Neuron*, **59**, 882–901 (2008). DOI: S0896-6273(08)00752-6 [pii] 10.1016/j.neuron.2008.09.005.
23. DB Halling, DK Georgiou, DJ Black, G Yang, JL Fallon, FA Quiocho, SE Pedersen and SL Hamilton, *J Biol Chem*, (2009). DOI: M109.013326 [pii] 10.1074/jbc.M109.013326.
24. F Van Petegem, FC Chatelain and DL Minor Jr, *Nat Struct Mol Biol*, **12**, 1108–15 (2005).
25. JL Fallon, DB Halling, SL Hamilton and FA Quiocho, *Structure*, **13**, 1881–86 (2005).
26. EY Kim, CH Rumpf, Y Fujiwara, ES Cooley, F Van Petegem and DL Minor Jr, *Structure*, **16**, 1455–67 (2008).
27. MX Mori, CW Vander Kooi, DJ Leahy and DT Yue, *Structure*, **16**, 607–20 (2008).
28. F Van Petegem and DL Minor, *Biochem Soc Trans*, **34**, 887–93 (2006).
29. AC Dolphin, *J Bioenerg Biomembr*, **35**, 599–620 (2003).
30. A Davies, J Hendrich, AT Van Minh, J Wratten, L Douglas and AC Dolphin, *Trends Pharmacol Sci*, **28**, 220–28 (2007).
31. GS Pitt, *Cardiovasc Res*, **73**, 641–47 (2007).
32. K Dunlap, *J Gen Physiol*, **129**, 379–83 (2007).
33. DB Halling, P Aracena-Parks and SL Hamilton, *Sci STKE*, **2006**, er1 (2006).
34. CD DeMaria, TW Soong, BA Alseikhan, RS Alvania and DT Yue, *Nature*, **411**, 484–89 (2001).
35. A Lee, H Zhou, T Scheuer and WA Catterall, *Proc Natl Acad Sci U S A*, **12**, 12 (2003).
36. H Liang, CD DeMaria, MG Erickson, MX Mori, BA Alseikhan and DT Yue, *Neuron*, **39**, 951–60 (2003).
37. BZ Peterson, CD DeMaria, JP Adelman and DT Yue, *Neuron*, **22**, 549–58 (1999).
38. F Van Petegem, KA Clark, FC Chatelain and DL Minor Jr, *Nature*, **429**, 671–75 (2004).
39. DE Clapham, *Cell*, **131**, 1047–58 (2007).
40. CB Klee, TH Crouch and PG Richman, *Annu Rev Biochem*, **49**, 489–515 (1980). DOI: 10.1146/annurev.bi.49.070180.002421.
41. A Crivici and M Ikura, *Annu Rev Biophys Biomol Struct*, **24**, 85–116 (1995).
42. S Nakayama and RH Kretsinger, *Annu Rev Biophys Biomol Struct*, **23**, 473–507 (1994). DOI: 10.1146/annurev.bb.23.060194.002353.
43. ZA Ataman, L Gakhar, BR Sorensen, JW Hell and MA Shea, *Structure*, **15**, 1603–17 (2007).
44. R Fischer, M Koller, M Flura, S Mathews, MA Strehler-Page, J Krebs, JT Penniston, E Carafoli and EE Strehler, *J Biol Chem*, **263**, 17055–62 (1988).
45. JT Littleton and B Ganetzky, *Neuron*, **26**, 35–43 (2000). DOI: S0896-6273(00)81135-6 [pii].
46. W Zheng, G Feng, D Ren, DF Eberl, F Hannan, M Dubald and LM Hall, *J Neurosci*, **15**, 1132–43 (1995).

47. RY Lee, L Lobel, M Hengartner, HR Horvitz and L Avery, *EMBO J*, **16**, 6066–76 (1997).
48. WR Schafer and CJ Kenyon, *Nature*, **375**, 73–78 (1995). DOI: 10.1038/375073a0.
49. D Zoccola, E Tambutte, F Senegas-Balas, JF Michiels, JP Failla, J Jaubert and D Allemand, *Gene*, **227**, 157–67 (1999).
50. MC Jeziorski, RM Greenberg, KS Clark and PA Anderson, *J Biol Chem*, **273**, 22792–99 (1998).
51. SL Hamilton, II Serysheva, *J Biol Chem*, **284**, 4047–51 (2009). DOI: R800054200 [pii] 10.1074/jbc.R800054200.
52. A Marcantoni, P Baldelli, JM Hernandez-Guijo, V Comunanza, V Carabelli and E Carbone, *Cell Calcium*, **42**, 397–408 (2007). DOI: S0143-4160(07)00101-7 [pii] 10.1016/j.ceca.2007.04.015.
53. SN Yang and PO Berggren, *Endocr Rev*, **27**, 621–76 (2006). DOI: er.2005-0888 [pii] 10.1210/er.2005-0888.
54. J Striessnig, A Koschak, MJ Sinnegger-Brauns, A Hetzenauer, NK Nguyen, P Busquet, G Pelster and N Singewald, *Biochem Soc Trans*, **34**, 903–9 (2006). DOI: BST0340903 [pii] 10.1042/BST0340903.
55. J Striessnig, HJ Bolz and A Koschak, *Pflugers Arch*, (2010). DOI: 10.1007/s00424-010-0800-x.
56. CJ Doering, JB Peloquin and JE McRory, *Channels (Austin)*, **1**, 3–10 (2007). DOI: 3938 [pii].
57. RM Evans and GW Zamponi, *Trends Neurosci*, **29**, 617–24 (2006).
58. P Liao, HY Zhang and TW Soong, *Pflugers Arch*, **458**, 481–87 (2009). DOI: 10.1007/s00424-009-0635-5.
59. AC Gray, J Raingo and D Lipscombe, *Cell Calcium*, **42**, 409–17 (2007). DOI: S0143-4160(07)00076-0 [pii] 10.1016/j.ceca.2007.04.003.
60. P Liao and TW Soong, *Pflugers Arch*, **460**(2), 353–9 (2010). DOI: 10.1007/s00424-009-0753-0.
61. D Pietrobon, *Pflugers Arch*, **460**(2), 375–93 (2010). DOI: 10.1007/s00424-010-0802-8.
62. DJ Triggle, *Curr Pharm Des*, **12**, 443–57 (2006).
63. DJ Triggle, *Biochem Pharmacol*, **74**, 1–9 (2007).
64. E Bourinet and GW Zamponi, *Curr Top Med Chem*, **5**, 539–46 (2005).
65. CJ Doering and GW Zamponi, *J Bioenerg Biomembr*, **35**, 491–505 (2003).
66. JP Benitah, AM Gomez, J Fauconnier, BG Kerfant, E Perrier, G Vassort and S Richard, *Basic Res Cardiol*, **97**, I11–18 (2002).
67. AA Grace and AJ Camm, *Cardiovasc Res*, **45**, 43–51 (2000).
68. AA Kochegarov, *Cell Calcium*, **33**, 145–62 (2003).
69. DJ Dooley, CP Taylor, S Donevan and D Feltner, *Trends Pharmacol Sci*, **28**, 75–82 (2007).
70. KS Elmslie, *J Neurosci Res*, **75**, 733–41 (2004).
71. N Klugbauer, E Marais and F Hofmann, *J Bioenerg Biomembr*, **35**, 639–47 (2003).
72. TN Davis, MS Urdea, FR Masiarz and J Thorner, *Cell*, **47**, 423–31 (1986). DOI: 0092-8674(86)90599-4 [pii].
73. EJ Wawrzynczak and RN Perham, *Biochem Int*, **9**, 177–85 (1984).
74. WE Zimmer, JA Schloss, CD Silflow, J Youngblom and DM Watterson, *J Biol Chem*, **263**, 19370–83 (1988).
75. V Ling, I Perera and RE Zielinski, *Plant Physiol*, **96**, 1196–202 (1991).
76. MC Gawienowski, D Szymanski, IY Perera and RE Zielinski, *Plant Mol Biol*, **22**, 215–25 (1993).
77. K Hogan, PA Powers and RG Gregg, *Genomics*, **24**, 608–9 (1994). DOI: S0888-7543(84)71677-6 [pii] 10.1006/geno.1994.1677.
78. P Ruth, A Rohrkasten, M Biel, E Bosse, S Regulla, HE Meyer, V Flockerzi and F Hofmann, *Science*, **245**, 1115–18 (1989).
79. T Tanabe, H Takeshima, A Mikami, V Flockerzi, H Takahashi, K Kangawa, M Kojima, H Matsuo, T Hirose and S Numa, *Nature*, **328**, 313–18 (1987). DOI: 10.1038/328313a0.
80. NM Soldatov, *Proc Natl Acad Sci U S A*, **89**, 4628–32 (1992).
81. NM Soldatov, A Bouron and H Reuter, *J Biol Chem*, **270**, 10540–43 (1995).
82. RD Zuhlke, A Bouron, NM Soldatov and H Reuter, *FEBS Lett*, **427**, 220–24 (1998). DOI: S0014-5793(98)00425-6 [pii].
83. ME Williams, DH Feldman, AF McCue, R Brenner, G Velicelebi, SB Ellis and MM Harpold, *Neuron*, **8**, 71–84 (1992). DOI: 0896-6273(92)90109-Q [pii].
84. S Seino, L Chen, M Seino, O Blondel, J Takeda, JH Johnson and GI Bell, *Proc Natl Acad Sci U S A*, **89**, 584–88 (1992).
85. TM Strom, G Nyakatura, E Apfelstedt-Sylla, H Hellebrand, B Lorenz, BH Weber, K Wutz, N Gutwillinger, K Ruther, B Drescher, C Sauer, E Zrenner, T Meitinger, A Rosenthal and A Meindl, *Nat Genet*, **19**, 260–63 (1998).
86. M Hans, A Urrutia, C Deal, PF Brust, K Stauderman, SB Ellis, MM Harpold, EC Johnson and ME Williams, *Biophys J*, **76**, 1384–400 (1999). DOI: S0006-3495(99)77300-5 [pii] 10.1016/S0006-3495(99)77300-5.
87. Y Mori, T Friedrich, MS Kim, A Mikami, J Nakai, P Ruth, E Bosse, F Hofmann, V Flockerzi, T Furuichi, K Mikoshiba, K Imoto, T Tanabe and S Numa, *Nature*, **350**, 398–402 (1991). DOI: 10.1038/350398a0.
88. ME Williams, PF Brust, DH Feldman, S Patthi, S Simerson, A Maroufi, AF McCue, G Velicelebi, SB Ellis and MM Harpold, *Science*, **257**, 389–95 (1992).
89. Y Fujita, M Mynlieff, RT Dirksen, MS Kim, T Niidome, J Nakai, T Friedrich, N Iwabe, T Miyata and T Furuichi, D Furutama, K Mikoshiba, Y Mori and KG Beam, *Neuron*, **10**, 585–98 (1993). DOI: 0896-6273(93)90162-K [pii].
90. T Schneider, X Wei, R Olcese, JL Costantin, A Neely, P Palade, E Perez-Reyes, N Qin, J Zhou and GD Crawford, *Recept Channels*, **2**, 255–70 (1994).
91. TW Soong, A Stea, CD Hodson, SJ Dubel, SR Vincent and TP Snutch, *Science*, **260**, 1133–36 (1993).
92. S Mittman, J Guo and WS Agnew, *Neurosci Lett*, **274**, 143–46 (1999). DOI: S0304394099007168 [pii].
93. E Perez-Reyes, LL Cribbs, A Daud, AE Lacerda, J Barclay, MP Williamson, M Fox, M Rees and JH Lee, *Nature*, **391**, 896–900 (1998). DOI: 10.1038/36110.
94. LL Cribbs, JH Lee, J Yang, J Satin, Y Zhang, A Daud, J Barclay, MP Williamson, M Fox, M Rees and E Perez-Reyes, *Circ Res*, **83**, 103–9 (1998).
95. S Mittman, J Guo, MC Emerick and WS Agnew, *Neurosci Lett*, **269**, 121–24 (1999). DOI: S0304394099003195 [pii].
96. JH Lee, AN Daud, LL Cribbs, AE Lacerda, A Pereverzev, U Klockner, T Schneider and E Perez-Reyes, *J Neurosci*, **19**, 1912–21 (1999).
97. II Serysheva, SJ Ludtke, MR Baker, W Chiu and SL Hamilton, *Proc Natl Acad Sci U S A*, **99**, 10370–75 (2002).
98. MC Wang, G Velarde, RC Ford, NS Berrow, AC Dolphin and A Kitmitto, *J Mol Biol*, **323**, 85–98 (2002).
99. M Wolf, A Eberhart, H Glossmann, J Striessnig and N Grigorieff, *J Mol Biol*, **332**, 171–82 (2003).

100. MC Wang, RF Collins, RC Ford, NS Berrow, AC Dolphin and A Kitmitto, *J Biol Chem*, **279**, 7159–68 (2004). DOI: 10.1074/jbc.M308057200 M308057200 [pii].
101. http://www.pymol.org/.
102. RB Kapust, J Tozser, JD Fox, DE Anderson, S Cherry, TD Copeland and DS Waugh, *Protein Eng*, **14**, 993–1000 (2001).
103. R Gopalakrishna and WB Anderson, *Biochem Biophys Res Commun*, **104**, 830–36 (1982). DOI: 0006-291X(82)90712-4 [pii].
104. M Zhang, T Tanaka and M Ikura, *Nat Struct Biol*, **2**, 758–67 (1995).
105. H Kuboniwa, N Tjandra, S Grzesiek, H Ren, CB Klee and A Bax, *Nat Struct Biol*, **2**, 768–76 (1995).
106. J Trewhella, *Cell Calcium*, **13**, 377–90 (1992).
107. G Barbato, M Ikura, LE Kay, RW Pastor and A Bax, *Biochemistry*, **31**, 5269–78 (1992).
108. MA Wilson and AT Brunger, *J Mol Biol*, **301**, 1237–56 (2000). DOI: 10.1006/jmbi.2000.4029 S0022-2836(00)94029-4 [pii].
109. JL Fallon and FA Quiocho, *Structure*, **11**, 1303–7 (2003). DOI: S0969212603002053 [pii].
110. RH Kretsinger and CE Nockolds, *J Biol Chem*, **248**, 3313–26 (1973).
111. JJRF da Silva and RJP Williams, *The Biological Chemistry of the Elements*, Oxford University Press, Oxford (1991).
112. S Ohki, M Ikura and M Zhang, *Biochemistry*, **36**, 4309–16 (1997). DOI: 10.1021/bi962759m bi962759m [pii].
113. SR Martin, L Masino and PM Bayley, *Protein Sci*, **9**, 2477–88 (2000). DOI: 10.1110/ ps.9.12.2477.
114. S Linse, A Helmersson and S Forsen, *J Biol Chem*, **266**, 8050–54 (1991).
115. P Bayley, P Ahlstrom, SR Martin and S Forsen, *Biochem Biophys Res Commun*, **120**, 185–91 (1984). DOI: 0006-291X(84)91431-1 [pii].
116. A Teleman, T Drakenberg and S Forsen, *Biochim Biophys Acta*, **873**, 204–13 (1986). DOI: 0167-4838(86)90047-6 [pii].
117. PM Bayley, WA Findlay and SR Martin, *Protein Sci*, **5**, 1215–28 (1996). DOI: 10.1002/pro.5560050701.
118. TS Ulmer, S Soelaiman, S Li, CB Klee, WJ Tang and A Bax, *J Biol Chem*, **278**, 29261–66 (2003). DOI: 10.1074/jbc.M302837200 M302837200 [pii].
119. CY Huang, V Chau, PB Chock, JH Wang and RK Sharma, *Proc Natl Acad Sci U S A*, **78**, 871–74 (1981).
120. NT Theoharis, BR Sorensen, J Theisen-Toupal and MA Shea, *Biochemistry*, **47**, 112–23 (2008). DOI: 10.1021/bi7013129.
121. TR Gaertner, JA Putkey and MN Waxham, *J Biol Chem*, **279**, 39374–82 (2004). DOI: 10.1074/jbc.M405352200 M405352200 [pii].
122. JA Putkey, Q Kleerekoper, TR Gaertner and MN Waxham, *J Biol Chem*, **278**, 49667–70 (2003). DOI: 10.1074/jbc.C300372200 C300372200 [pii].
123. JA Putkey, MN Waxham, TR Gaertner, KJ Brewer, M Goldsmith, Y Kubota and QK Kleerekoper, *J Biol Chem*, **283**, 1401–10 (2008). DOI: M703831200 [pii] 10.1074/jbc.M703831200.
124. JD Johnson, C Snyder, M Walsh and M Flynn, *J Biol Chem*, **271**, 761–67 (1996).
125. BB Olwin and DR Storm, *Biochemistry*, **24**, 8081–86 (1985).
126. DJ Black, DB Halling, DV Mandich, SE Pedersen, RA Altschuld and SL Hamilton, *Am J Physiol Cell Physiol*, **288**, C669–76 (2005).
127. AR Rhoads and F Friedberg, *Biochem J*, **11**, 331–40 (1997).
128. M Bahler and A Rhoads, *FEBS Lett*, **513**, 107–13 (2002).
129. LA Jurado, PS Chockalingam and HW Jarrett, *Physiol Rev*, **79**, 661–82 (1999).
130. GS Pitt, RD Zühlke, A Hudmon, H Schulman, H Reuter and RW Tsien, *J Biol Chem*, **276**, 30794–802 (2001).
131. N Qin, R Olcese, M Bransby, T Lin and L Birnbaumer, *Proc Natl Acad Sci U S A*, **96**, 2435–38 (1999).
132. RD Zühlke, GS Pitt, K Deisseroth, RW Tsien and H Reuter, *Nature*, **399**, 159–62 (1999).
133. H Kurokawa, M Osawa, H Kurihara, N Katayama, H Tokumitsu, MB Swindells, M Kainosho and M Ikura, *J Mol Biol*, **312**, 59–68 (2001).
134. M Osawa, H Tokumitsu, MB Swindells, H Kurihara, M Orita, T Shibanuma, T Furuya and M Ikura, *Nat Struct Biol*, **6**, 819–24 (1999).
135. RD Zühlke, GS Pitt, RW Tsien and H Reuter, *J Biol Chem*, **275**, 21121–29 (2000).
136. W Tang, DB Halling, DJ Black, P Pate, JZ Zhang, S Pedersen, RA Altschuld and SL Hamilton, *Biophys J*, **85**, 1538–47 (2003).
137. MF Schneider and WK Chandler, *Nature*, **242**, 244–46 (1973).
138. E Rios and G Brum, *Nature*, **325**, 717–20 (1987). DOI: 10.1038/325717a0.
139. J Schredelseker, M Shrivastav, A Dayal and M Grabner, *Proc Natl Acad Sci U S A*, **107**, 5658–63 (2010). DOI: 0912153107 [pii] 10.1073/pnas.0912153107.
140. CM Wilkens, N Kasielke, BE Flucher, KG Beam and M Grabner, *Proc Natl Acad Sci U S A*, **98**, 5892–97 (2001). DOI: 10.1073/pnas.101618098 101618098 [pii].
141. C Proenza, CM Wilkens and KG Beam, *J Biol Chem*, **275**, 29935–37 (2000). DOI: 10.1074/jbc.C000464200 C000464200 [pii].
142. K Stroffekova, *Pflugers Arch*, **455**, 873–84 (2008). DOI: 10.1007/s00424-007-0344-x.
143. J Ohrtman, B Ritter, A Polster, KG Beam and S Papadopoulos, *J Biol Chem*, **283**, 29301–11 (2008). DOI: M805152200 [pii] 10.1074/jbc.M805152200.
144. MG Erickson, BA Alseikhan, BZ Peterson and DT Yue, *Neuron*, **31**, 973–85 (2001).
145. MG Erickson, H Liang, MX Mori and DT Yue, *Neuron*, **39**, 97–107 (2003).
146. LY Lian, D Myatt and A Kitmitto, *Biochem Biophys Res Commun*, **353**, 565–70 (2007).
147. HG Wang, MS George, J Kim, C Wang and GS Pitt, *J Neurosci*, **27**, 9086–93 (2007). DOI: 27/34/9086 [pii] 10.1523/JNEUROSCI.1720-07.2007.
148. MR Tadross, IE Dick and DT Yue, *Cell*, **133**, 1228–40 (2008).
149. J Kim, S Ghosh, DA Nunziato and GS Pitt, *Neuron*, **41**, 745–54 (2004).
150. C Romanin, R Gamsjaeger, H Kahr, D Schaufler, O Carlson, DR Abernethy and NM Soldatov, *FEBS Lett*, **487**, 301–6 (2000).
151. M de Leon, Y Wang, L Jones, E Perez-Reyes, X Wei, TW Soong, TP Snutch and DT Yue, *Science*, **270**, 1502–6 (1995).
152. IE Dick, MR Tadross, H Liang, LH Tay, W Yang and DT Yue, *Nature*, **451**, 830–34 (2008).
153. T Ivanina, Y Blumenstein, E Shistik, R Barzilai and N Dascal, *J Biol Chem*, **275**, 39846–54 (2000).
154. A Lee, ST Wong, D Gallagher, B Li, DR Storm, T Scheuer and WA Catterall, *Nature*, **399**, 155–59 (1999).
155. JT Hulme, V Yarov-Yarovoy, TW Lin, T Scheuer and WA Catterall, *J Physiol*, **576**, 87–102 (2006).

156. A Singh, D Hamedinger, JC Hoda, M Gebhart, A Koschak, C Romanin and J Striessnig, *Nat Neurosci*, **9**, 1108–16 (2006).
157. C Wahl-Schott, L Baumann, H Cuny, C Eckert, K Griessmeier and M Biel, *Proc Natl Acad Sci U S A*, **103**, 15657–62 (2006).
158. F Findeisen, DL Minor Jr, *J Gen Physiol*, **133**, 327–43 (2009). DOI: jgp.200810143 [pii] 10.1085/jgp.200810143.
159. T Cens, M Rousset, JP Leyris, P Fesquet and P Charnet, *Prog Biophys Mol Biol*, **90**, 104–17 (2006).
160. W Yuan and DM Bers, *Am J Physiol*, **267**, H982–93 (1994).
161. ME Anderson, AP Braun, H Schulman and BA Premack, *Circ Res*, **75**, 854–61 (1994).
162. A Hudmon, H Schulman, J Kim, JM Maltez, RW Tsien and GS Pitt, *J Cell Biol*, **171**, 537–47 (2005).
163. CE Grueter, SA Abiria, I Dzhura, Y Wu, AJ Ham, PJ Mohler, ME Anderson and RJ Colbran, *Mol Cell*, **23**, 641–50 (2006).
164. TS Lee, R Karl, S Moosmang, P Lenhardt, N Klugbauer, F Hofmann, T Kleppisch and A Welling, *J Biol Chem*, **281**, 25560–67 (2006).
165. X Jiang, NJ Lautermilch, H Watari, RE Westenbroek, T Scheuer and WA Catterall, *Proc Natl Acad Sci U S A*, **105**, 341–46 (2008).